32nd International Cosmic Ray Conference, Beijing 2011

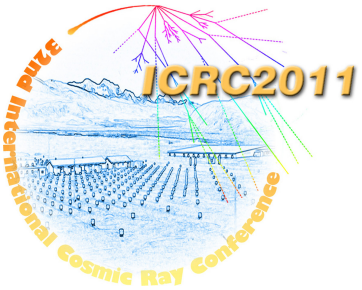

Recent Results and the next step of the Tibet ASγ experiment

J. Huang on behalf of The Tibet ASγ Collaboration[1)]

Key Laboratory of Particle Astrophysics, Institute of High Energy Physics,
Chinese Academy of Sciences, Beijing 100049, China

Abstract: The Tibet-III air-shower array has been operating successfully at Yangbajing (E90°31′, N30°06′; 4300 m above sea level) in Tibet, China, since 2003, producing many new results related to high energy cosmic ray physics. Recently, we started to construct an underground water Cherenkov muon detector (MD) array and a burst detector (YAC) array within the area of the Tibet-III AS array. This detector-array complex is able to observe air showers of high energy celestial gamma-ray origin and those of nuclear-component origin with considerable accuracy. In this paper, we briefly present some results recently obtained with the Tibet-III air-shower array and also introduce the status of our future plans which are called the Tibet (AS+MD) project and Tibet (AS+YAC+MD) project.

Key words: Tibet, cosmic ray, knee, air shower, TeV gamma rays, solar modulation, Sun's shadow, anisotropy

1 Introduction

The Tibet air-shower experiment has been operated at Yangbajing (E90°31′, N30°06′; 4300 m above sea level) in Tibet, China, since 1990. The Tibet air-shower array is designed not only for observation of air showers of nuclear-component origin but also for that of high energy celestial gamma rays. Because of such multiple purposes, the detector is constructed to cover a wide dynamic range for particle density covering 0.1 to 5000 and a good angular resolution for the arrival direction of air showers with energy in excess of a few TeV being better than 1 degree.

The Tibet-I surface array was constructed in 1990 using 65 plastic scintillation detectors placed on a lattice with 15 m spacing. This array was gradually expanded to the Tibet-II (1994) and Tibet-III (1999) array. At present, it consists of 761 fast timing (FT) counters and 28 density (D) counters surrounding them (Figure 1). In the inner 36,900 m^2, FT counters are deployed at 7.5 m lattice intervals. All the FT counters are equipped with a fast-timing photomultiplier tube (FT-PMT; Hamamatsu H1161) measuring up to 15 particles. Among the 761 FT counters, 249 sets of detectors (with interval of 15 m) are also equipped with density photomultiplier tube (D-PMT; Hamamatsu H3178) of wide dynamic range measuring up to 5000 particles in addition to FT-PMTs, so that UHE cosmic rays with energy above the knee can be observed with a good accuracy.

Each counter has a plastic scintillator plate (BICRON BC-408A) of 0.5 m^2 in area and 3 cm in thickness. A lead plate of 0.5 cm thick is put on the top of each counter, in order to increase the counter's sensitivity by converting photons in an electromagnetic shower into electron-positron pairs. The recording of signals is made on time and charge information for the FT-PMTs, while only the charge information for the D-PMTs. The D counters surrounding the inner array are also equipped with both FT-PMT and D-PMT, where only the charge information of both PMTs are recorded. An event trigger signal is issued when any fourfold coincidence occurs in the FT counters recording more than 0.6 particles. The number of air shower particles and the arrival timing of particles at each detector are recorded, allowing us to estimate primary cosmic ray or γ-ray direction and energy for each air shower. Figure 1 is the schematic view of the

1) E-mail: huangjing@ihep.ac.cn

DOI: 10.7529/ICRC2011/V12/H08

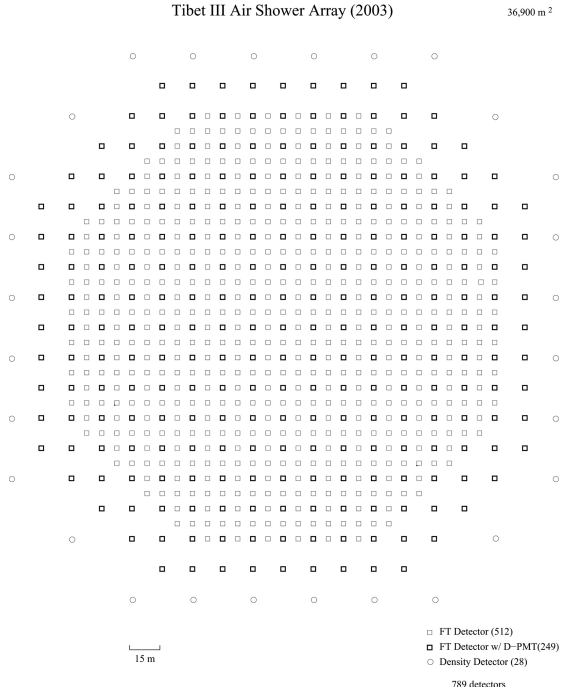

Fig. 1. Schematic view of the Tibet-III array operating at Yangbajing.

Tibet-III array.

The primary energy of each event is determined by the shower size N_e, which is calculated by fitting the lateral particle density distribution to the modified NKG structure function [1]. The performance of the Tibet air shower array has been well examined by observing the Moon's shadow (approximately 0.5 degree arc in diameter) in cosmic rays [2]. The deficit map of cosmic rays around the Moon demonstrates the angular resolution to be around 0.9 degree at a few TeV for the Tibet-III array. The pointing error is estimated to be less than ∼0.01 degree by displacement of the shadow's center from the apparent center in the north-south direction, as the east-west component of the geomagnetic field is very small at the experimental site. On the other hand, the shadow center displacement in the east-west direction due to the geomagnetic field enables us to spectroscopically estimate the energy scale uncertainty less than ±12% [2].

We observe cosmic rays and γ-rays using the above-mentioned Tibet-III array with a duty cycle of about 24 hr every day regardless of weather conditions and with a wide field of view of about 2 sr. These capabilities give us an unbiased survey of the northern sky.

Using the Tibet-III and previous arrays, we have successfully observed TeV γ-ray sources, such as the Crab Nebula, Mrk 501, and Mrk 421. We have also successfully obtained the all-particle spectrum of primary cosmic rays in the wide energy range from 10^{14} to 10^{17} eV, which is the highest statistical and the best systematics-controlled measurement covering the widest energy range around the knee energy region in the world [1]. We have also successfully drawn a precise two-dimensional map of the large-scale cosmic-ray anisotropy in the northern sky [3], where we first point out new small-area enhancements in the Cygnus arm direction at multi-TeV energies. One of the enhancements is coincident with MGRO J2019+37, which was established recently by the Milagro experiment as a TeV γ-ray source [4]. It is worth noting that the Tibet ASγ experiment has reported several times [5,6] on the marginal excesses from the direction closing to MGRO J1908+06/HESS J1908+063 before the final discovery made by the Milagro experiment.

In this paper, I would like to report our recent results and the next step of the Tibet ASγ experiment.

2 TeV gamma ray astronomy

Recently, using the Tibet-III air shower array, we search for TeV γ-rays from 27 potential Galactic sources in the early list of bright sources obtained by the *Fermi* Large Area Telescope at energies above 100 MeV [7]. Among them, we observe seven sources instead of the expected 0.61 sources at a significance of 2σ or more excess. The chance probability from Poisson statistics would be estimated to be 3.8×10^{-6} . If the excess distribution observed by the Tibet-III array has a density gradient toward the Galactic plane, the expected number of sources may be enhanced in chance association. Then, the chance probability rises slightly, to 1.2×10^{-5}, based on a simple Monte Carlo simulation. These low chance probabilities clearly show that the *Fermi* bright Galactic sources have statistically significant correlations with TeV γ-ray excesses. We also find that all seven sources are associated with pulsars, and six of them are coincident with sources detected by the Milagro experiment at a significance of 3σ or more at the representative energy of 35 TeV. The significance maps observed by the Tibet-III air shower array around the *Fermi* sources, which are coincident with the Milagro $\geq 3\sigma$ sources, are consistent with the Milagro observations as shown in Figure 2. This is the first result of the northern sky survey of the *Fermi* bright Galactic sources in the TeV region.

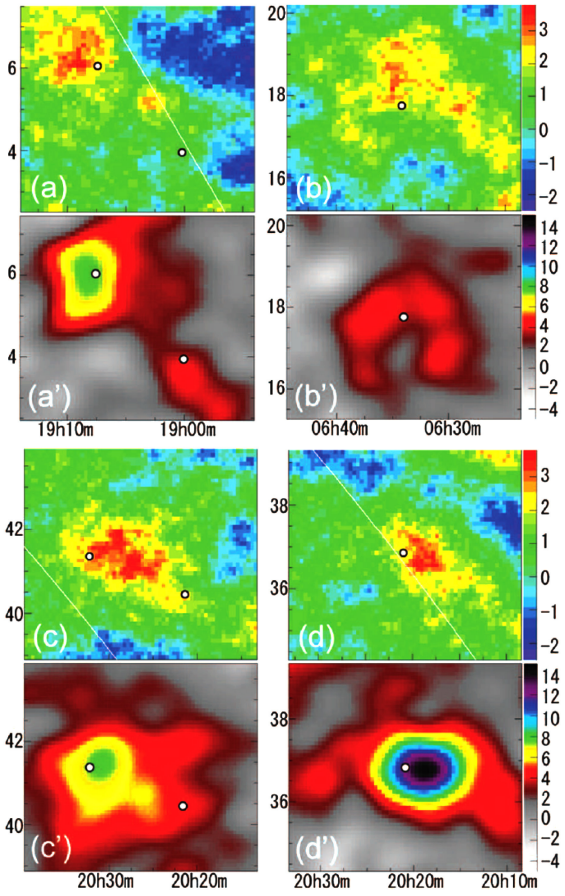

Fig. 2. Comparisons of significance maps around the *Fermi* sources between the Tibet-III array (a)-(d) and the Milagro experiment (a')-(d') taken from Abdo et al. [4]. Selected are *Fermi* source with $\leq 2\sigma$ significance by the Tibet-III array and $\leq 3\sigma$ by the Milagro experiment except for the Crab. White points in each image show the *Fermi* source positions: (a and a') J1907.5+0602/J1900.0+0356; (b and b') J0634.0+1745 (Geminga); (c and c') J2021.5+4026/J2032.2+4122; (d and d') J2020.8+3649. The horizontal axis, vertical axis, and color contours indicate the right ascension, declination, and significance, respectively.

3 Knee physics

A sudden steepening of the cosmic-ray energy spectrum around 4×10^{15} eV is called "knee" where the value of the power index γ changes from approximately 2.7 to 3.1 when the energy spectrum is express by a power law $\propto E^{-\gamma}$. The origin of the knee is discussed based on the result of Tibet air-shower experiment over the wide energy range from 10^{14} eV to 10^{17} eV covering the knee region [1]. There has been a lot of works on the origin of the knee in terms of the acceleration mechanism [8], the propagation in the Galaxy [9] or some nearby sources [10]. Another point of view is related to the nature of hadronic interactions [11].

In this work, for explaining the sharp knee we proposed two composition models which are called model A and model B, as shown in Figure 3 and Figure 4 [12], that are based on : 1) the up-to-now available experimental results; 2) some physics (or theoretical) assumptions. In model A, sharp knee is due to nearby sources whose chemical composition is dominated by nuclei heavier than helium. Consequently the dominance of heavy nuclei is limited to the energy region around the knee. On the other hand, in model B, sharp knee is due to nonlinear effects in the diffusive shock acceleration leading to iron-dominant composition at the knee and beyond.

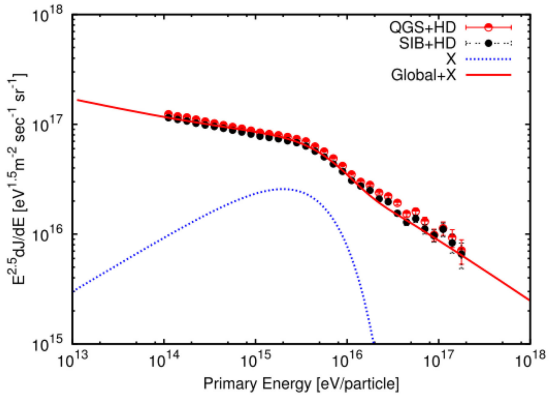

Fig. 3. Model A: sharp knee is attributed to extra component from nearby source.

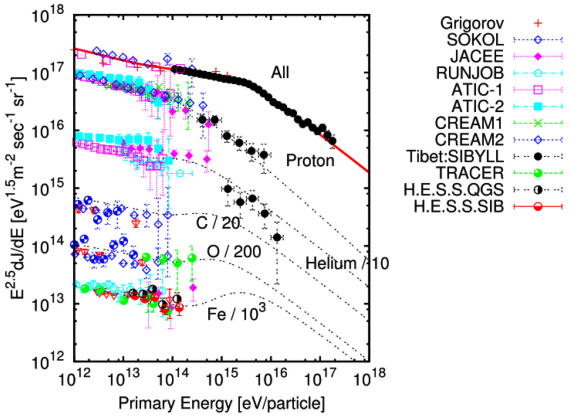

Fig. 4. Model B: nonlinear effect in the diffusive shock acceleration mechanism can explain the structure of the knee when high acceleration efficiency for heavy elements is assumed.

In order to distinguish between model A and model B and many other models, measurements of the chemical composition around the knee, especially measurements of the spectra of individual component till their knee will be essentially important.

Therefore, we planed a new experiment: 1) to lower down the energy measurement of individual component spectra to $\star$10 TeV and make connection with direct measurements; 2) to make a high precision measurement of primary p, He, c, Fe till 100 PeV region to see the rigidity cutoff effect. These aims will be realized by the new hybrid experiments YAC (Yangbajing AS Core array). The feature of the YAC experiment is described in Section 7.

4 The Sun's shadow in cosmic rays

High energy cosmic rays travel nearly straight in the interplanetary space between the Sun and the Earth. The Sun and Moon shield cosmic rays arriving from the directions behind them and cast tiny "shadows" in the directional intensity of cosmic rays observed at the Earth. The Sun's shadow has been of particular interest because it is expected to reflect the large-scale structure of the solar magnetic field near the Sun, which is still difficult to observe with direct and/or remote measurements.

In this work, we analyze the solar cycle variation of the Sun's shadow in 10 TeV cosmic ray intensity observed with the Tibet air shower array over an entire period of the Solar Cycle 23 between 1996 and 2008 [13], it shows that a clear solar cycle variation in a sense that the shadow is clear (faint) during the solar activity minimum (maximum) period as shown in Figure 5a and 5b. The amplitude of the variation is as large as 50% of the deficit intensity expected when all cosmic rays from the direction of the optical Sun disk are excluded from the observation. Among the solar cycle variations of GCR modulation parameters, we find the highest correlation ($\gamma = +0.94$) between the Sun's shadow and the HCS tilt-angle as shown in Figure 6a, 6b and 6c.

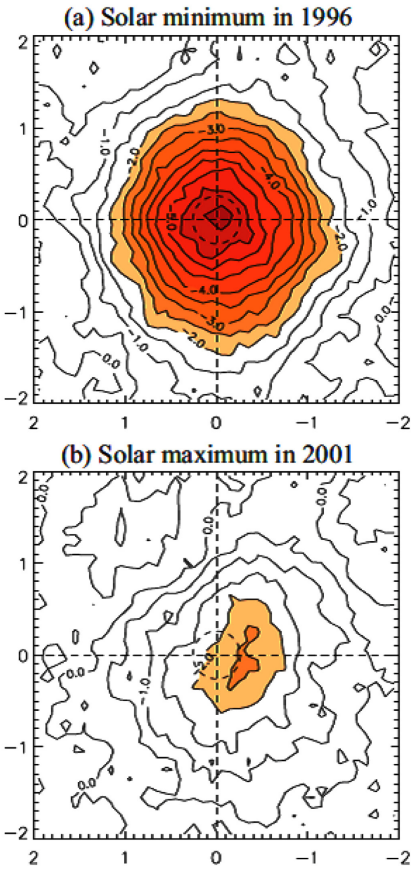

Fig. 5. Two dimensional maps of the observed Sun's shadow (a) in the solar minimum (1996), and (b) in the solar maximum (2001) at 10 TeV. Each panel disolays a counter map of the observed deficit intensity in the Sun's shadow in each year as a function of the GSE longitude and latitude.

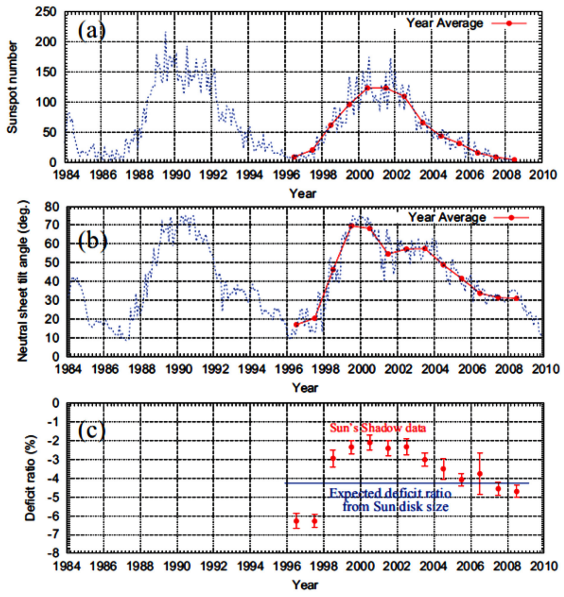

Fig. 6. Solar cycle variations of the GCR modulation parameters and the Sun's shadow at 10 TeV. The solid circles in each panel from the top displays the yearly mean value of (a) the sunspot number[14], (b) the HCS tilt-angle in degree [15] and (c) yearly mean deficit intensity observed in the Sun's shadow. Solid line in panel (c) indicate the expected deficit ratio when all cosmic rays from the direction of the optical Sun disk are excluded from the observation.

The solar activity is presently going toward the solar maximum expected in 2013. The observation of the Sun's shadow in next solar cycle is very important to see the solar modulation change in the solar activity and magnetic-cycles.

5 Cosmic-ray anisotropy

5.1 Modeling of the galactic cosmic-ray anisotropy at TeV energies

Past cosmic-ray experiments that observed cosmic-ray anisotropy in the sidereal time frame consistently reported that in the anisotropy there are two distinct broad structures with an amplitude of ∼0.1%; one is a deficit in the cosmic-ray flux called "loss-cone", distribute around 150° to 240° in Right Ascension, and the another excess called "tail-in", distributed around 40° to 90° in Right Ascension. Recent underground muon and air-shower experiments are studying the anisotropy in a great detail at multi-TeV energies [3,16]. It is considered that the anisotropy of galactic cosmic rays at TeV energies reflects the structure of the local interstellar magnetic field surrounding the heliosphere, since the trajectories of charged cosmic rays are deflected and scrambled by the local interstellar magnetic field while they are traveling through the interstellar medium.

Based on this, we discussed the origin of the large-scale anisotropy of galactic cosmic rays at TeV energies. It can be well modeled by a superposition of the Global Anisotropy and the Midscale Anisotropy [17]. The Global Anisotropy would be generated by galactic cosmic rays interacting with the magnetic field in the local interstellar space of a few parsec scale surrounding the heliosphere. On the other hand, the Midscale Anisotropy would be caused by the modulation of galactic cosmic rays in the heliotail. The Midscale Anisotropy can be expressed as two intensity enhancements placed along the Hydrogen Deflection Plane, each symmetrically centered away from the heliotail direction. It is found that the separation angle between the heliotail direction and each of the two intensity enhancement monotonously decreases as energy increases from 4 TeV to 30 TeV.

Figure 7 shows two-dimensional anisotropy maps of galactic cosmic rays observed and reproduced at the modal energy of 7 TeV. Each panel shows the relative intensity map or the significance map in 5° × 5° pixels in the equatorial coordinate system. A sketch of a possible mechanism for the Midscale Anisotropy is shown in Figure 8 [17].

5.2 Time dependence of Loss-Cone amplitude

The Milagro experiment in the U.S. detected a significant increase in the Loss-Cone amplitude at 6 TeV from July 2000 to July 2007, and argued that it could be due to variations in the heliosphere in

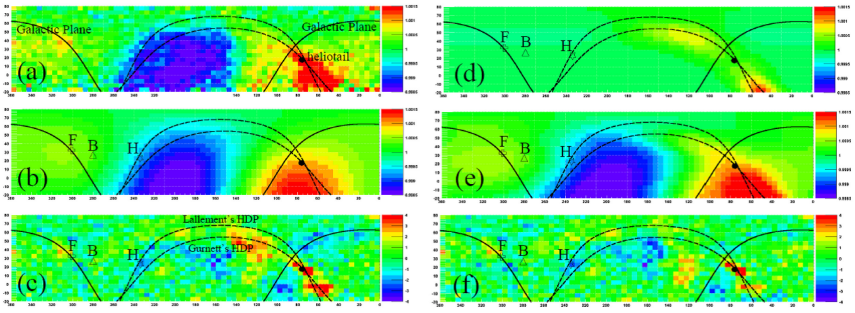

Fig. 7. Two-dimensional anisotropy maps of galactic cosmic rays observed and reproduced at the modal energy of 7 TeV. Each panel shows the relative intensity map or the significance map in 5° × 5° pixels in the equatorial coordinate system. (a): the observed cosmic-ray intensity ($I^{\rm obs}_{n,m}$), (b): the best-fit Global Anisotropy (GA) component ($I^{\rm GA}_{n,m}$), (c): the significance map of the residual anisotropy after subtracting ($I^{\rm GA}_{n,m}$ from ($I^{\rm obs}_{n,m}$), (d): the best-fit Midscale Anisotropy (MA) component ($I^{\rm MA}_{n,m}$), (e): the best-fit GA+MA components ($I^{\rm GA}_{n,m} + I^{\rm MA}_{n,m}$), (f): the significance map of the residual anisotropy after subtracting $I^{\rm GA}_{n,m} + I^{\rm MA}_{n,m}$ from $I^{\rm obs}_{n,m}$. The solid black curves represent the galatic plane. The dashed black curves represent the Hydrogen Deflection Plane reported by Gurnett at al. [18] and Lallement et al.[19]. The heliotail direction (α, δ) = (75.9°, 17.4°) is indicated by the black filled circle. The open cross and the inverted star with the attached characters "F" and "H" represent the orientation of the local interstellar magnetic field (LISMF) by Frisch [20] and by Heerikhuisen et al. [21], respectively. The open triangle with "B" indicates the orientation of the best-fit bi-directional cosmic-ray flow (BDF) [13].

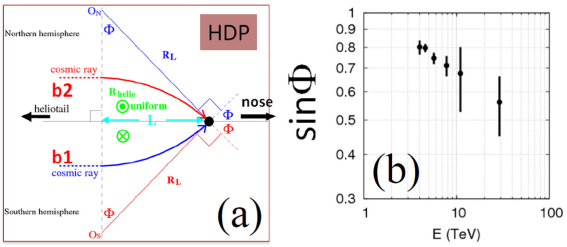

Fig. 8. (a): A possible mechanism for the Mid-scale Anisotropy; (b) the observed energy dependence of $\sin\phi$.

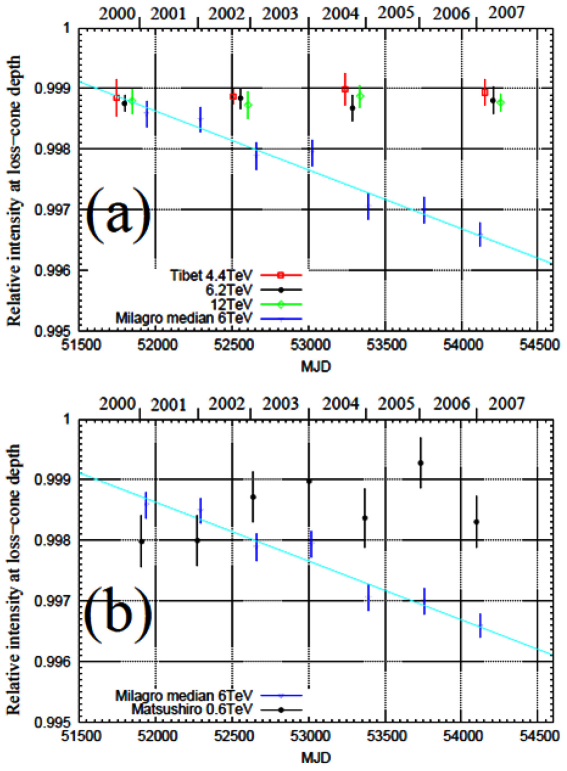

Fig. 9. Time dependence of the maximum depth of Loss-Cone observed by the Tibet experiment at 4.4, 6.2, 12 TeV (a) and the Matsushiro underground muon observatory at 0.6 TeV (b) [22], along with Milagro's data represented by blue open inverse triangles and the best-fit linear function to Milagro's data. The data and their errors by the Matsushiro underground muon observatory are multiplied by three, to compensate for the attenuation of the amplitude in the sub-TeV energy region. All the error bars in (a) and (b) are the linear sums of the statistical and systematic errors.

relation to solar activities. However, in this work, we report on the time dependence of the Loss-Cone amplitude from November 1999 through December 2008 measured with the Tibet air-shower array. No time dependence was found in the Loss-Cone amplitude at energies of 4.4, 6.2 and 11 TeV as shown in Figure 9a. If the increase in the Loss-Cone amplitude Milagro detected were genuine, the same tendency would be seen at sub-TeV energies where the anisotropy is far more sensitive to solar activities. Matsushiro underground muon observation at 0.6 TeV during the corresponding period, however, reported no significant increase of the Loss-Cone amplitude (Figure 9b).

5.3 Stable Multi-TeV anisotropy by ASγ experiment

In this work, we investigate temporal variations of the large-scale two-dimension sidereal anisotropy of multi-TeV cosmic rays (CRs) by the Tibet Air Shower Array, with the data taken from 1999 November to 2008 December [23]. To explore temporal variations of the anisotropy, the data set is divided into nine intervals, each with a time span of about one year. The sidereal anisotropy of magnitude, about 0.1%, appears fairly stable from year to year over the entire observation period of nine years as shown in Figure 10. This indicates that the anisotropy of TeV Galactic CRs remains insensitive to solar activities since the observation period covers more than half of the 23rd solar cycle.

5.4 Model based on the Anisotropy: contribution of the GCR to GMF

Based on the measured cosmic ray anisotropy, a model was built to calculate the contribution of the Galatic cosmic ray (GCR) to the large-scale Galactic magnetic field (GMF) as shown in Figure 11 [24]. A general agreement in the large-scale structure of the galactic magnetic field between the calculation and the observation was obtained. This result shows that the Galactic halo magnetic field may be partially contributed by the Galactic electric current related to the directional movement of cosmic rays and the model is the correct approach in understanding the possible contribution of cosmic rays to the galactic magnetic field. The model also indicates that the observed anisotropy of cosmic rays on the earth is not a local behavior in the solar vicinity but represents a microcosm of the global anisotropy of GCRs.

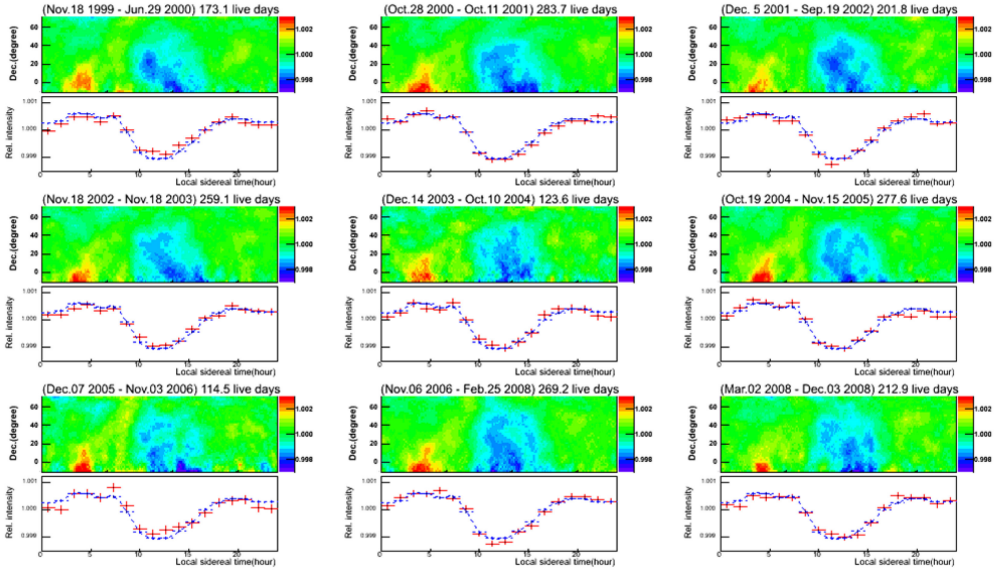

Fig. 10. CR intensity variation in the local sidereal time frame for CRs with the modal energy around 5 TeV in the nine phases of Tibet-III array. Top: two-dimensional intensity map of each phase; Bottom: one-dimensional projection averaged over all declinations. In bottom plots of each panel, the red crosses in each plot show the intensity variation over each phase respectively, while the dashed blue lines represent the intensity averaged over all nine phase of Tibet-III array.

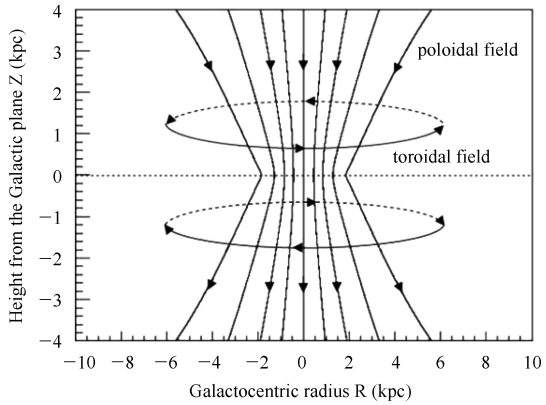

Fig. 11. Structure of the Galactic halo magnetic field contributed by the GCRs. The GMF in the halo is composed of a poloidal magnetic field and a toroidal magnetic field. The direction of the poloidal field is from Galactic north to south, passing through the disk plane. The toroidal field has reversed directions below and above the Galatic plane. The arrows indicate the directions of the magnetic fields.

6 Test of hadronic interaction models

The interpretation of the extensive air showers (EAS) is known to inevitably depend on the Monte Carlo simulations which are based on some hadronic interaction models and cosmic-ray composition models. At present, the simulation code CORSIKA that is comprehensively used in the surface cosmic-ray studies includes many interaction models. For multi-parameter measurements of EASs, it is known that no interaction model can explain all data consistently. Therefore, the hadronic interaction models need to be checked and further improved.

In this paper, we report our approach and the preliminary results to check the hadronic interaction models QGSJET2 and SIBYLL2.1 at an energy region of $\star$10 TeV using the data obtained by the newly constructed YAC-I (Yangbajing Air shower Core detector as the first stage, see Section 7). Data taking was made from May 2009 to February 2010. The energy region of $\star$10 TeV is chosen by the following considerations: 1) The primary composition at this energies has been better measured by direct measurements, and the uncertainty is smaller. 2) The corresponding energies in the center-of-mass system are around $\star$100 GeV where $p\bar{p}$ collider made good measurements on the inelastic cross section and on the particle production in the near-forward region. The uncertainty from the extrapolation to the very forward region is relatively small. 3) The check of interaction models should be step-by-step executed from lower energies to higher energies. 4) Due to the high altitude of our Tibet experiment we could have good EAS core events recorded by YAC-I at $\star$10 TeV region.

A small high-altitude AS core detector YAC-I (see Section 7) shows the ability and sensitivity in checking the hadronic interaction models in $\star$10 TeV region. In this work, two primary composition models are used, the heavy dominant model(HD)[1] and the non-linear acceleration model(NLA) [12]. The proton spectrum of the two models is connected with the direct experiment in the low energy and consistent with the spectrum obtained from the Tibet AS+EC experiment in the high energy. The He spectrum of HD model coincides with the results from RUNJOB and ATIC-I, but the He spectrum of NLA coincides with the results from JACEE, ATIC-II, CREAM3. The sum of all element's spectra can reproduce the sharp knee in all particle spectrum [12].

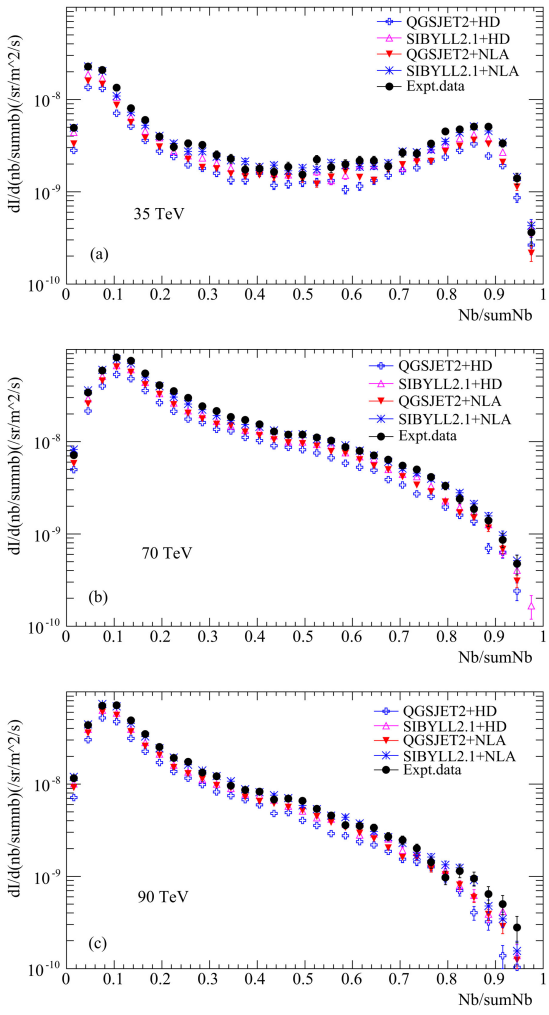

Fig. 12. The absolute intensity of $N_b/\sum N_b$ distribution of the three samples for QGSJET2+HD model, SIBYLL2.1+HD model, QGSJET2+NLA model, SIBYLL2.1+NLA model and the experimental data.

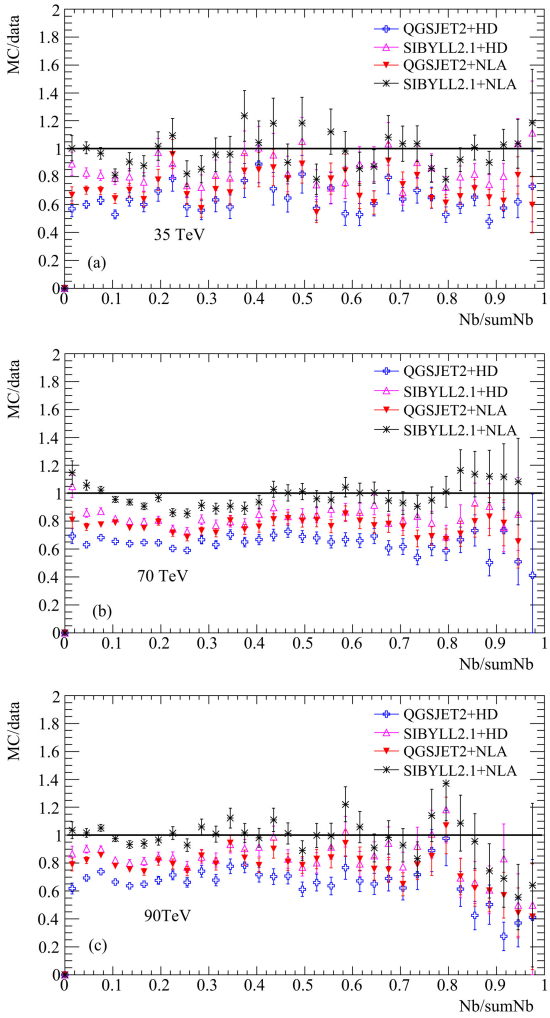

Fig. 13. The ratio of absolute intensity between MC and experiment data.

Following quantities of YAC-I are used to characterize an EAS core event: High-energy electromagnetic component (electrons and photons) at the EAS core induces cascade showers in lead absorber of the YAC detector (thickness of 7 r.l.). The number of shower electrons under the lead layer is measured by scintillator attached with photo tubes and called "burst size" (N_b). The conversion from PMT signal to particle number is calibrated by single muon peak. When the burst size of a detector unit is higher than 200, this unit is defined as a "fired" one. We also call the total burst size of all fired detector units as $\sum N_b$, the maximum burst size among fired detectors as $N_b^{\rm top}$. And then, we found the experimental distributions, $N_b/\sum N_b$ and has the shape very close to the Monte Carlo predictions of QGSJET2+NLA, QGSJET2+HD, SIBYLL2.1+NLA and SIBYLL2.1+HD as shown in

Figure 12a, 12b and 12c. Some other quantities, such as N_b, $\sum N_b$, $N_b^{\rm top}$, R_w, $R_w \times N_b$ have the same behavior as well, though we did not show them in this paper due to the limit of the space.

Some discrepancies in the absolute intensities are seen. Figure 13a, 13b and 13c show that data normally shows a higher intensity than Monte Carlo. Taking a more hard He spectrum (and somewhat hard proton spectrum) as given by CREAM [25] at the 1-100 TeV region can improve this situation. A further study is going on.

7 Project status and plan

As mentioned above, we found out that, 1) Crab, Mrk501, Mrk421 has been observed by using Tibet air-shower experiment, but no new steady bright TeV γ-ray point source is found, possible diffuse γ-ray signal from Cygnus region. 2) All particle spectrum was obtained by Tibet-III array in wide range of 10^{14}–10^{17} eV covering the knee and a sharp knee is observed at 4 PeV. P and He spectra in $10^{14}-10^{16}$ eV range were also obtained by AS+EC hybrid experiment showing that the knee is dominated by nuclei heavier than helium. New detectors are under construction aiming 1) 100 TeV (10-1000 TeV) region γ-ray astronomy (MD project) to answer the question "where galactic cosmic rays below the knee come from?" 2) detailed study of chemical composition around the "knee" (YAC project) which can provide key information on the cosmic-ray origin and the acceleration mechanism.

7.1 Tibet AS+MD Project

The HESS group with 4 large IACTs in Namibia reported on discovery of new 14 gamma-ray sources by galactic plane survey [26] in 2005. Surprisingly, most of them are UNIDentified (UNID) sources and faint in X-rays or other wavelengths. As the HESS survey was limited within the galactic plane in the southern hemisphere due to its narrow field of view, the importance of a wide field-of-view unbiased survey is emphasized. Furthermore, many of the 14 sources have a harder energy spectrum (indices: -1.8 to -2.8) at TeV energies than the standard candle Crab(index: -2.6). The energy spectra turned out to extend up to approximately 10 TeV. Cosmic rays are supposed to be accelerated up to the knee energy region at supernova remnants (SNRs) in our galaxy. Therefore, we naturally expect gamma rays in the 100 TeV region (10-1000 TeV) which originate in π^0 decays produced by the accelerated cosmic rays interacting with matter surrounding the SNRs. The gamma ray emission of electron origin might be highly suppressed in the 100 TeV region due to rapid decrease of inverse-Compton cross section by the Klein-Nishina effect as well as synchrotron radiation energy loss in the magnetic field around the SNRs. Multi-wavelength (radio, X-ray, gamma-ray) observations are essential to discriminate between the two processes.

To positively observe gamma rays in the 100 TeV region with much better sensitivity than Tibet-III array, we plan to add a muon detector array to the air-shower array. Gamma-ray induced electromagnetic air showers are muon-poor, while cosmic ray induced hadronic ones are accompanied by many muons. This enables us to separate gamma rays from cosmic rays. Our current plan [27] relevant to gamma-ray astronomy above 10 TeV is Tibet AS(Air Shower array with 83,000 m^2 in area) + MD (Muon Detector array with $\sim$ 10,000 m^2 in area under Tibet AS) as shown in Figure 14. Each muon detector is a waterproof concrete pool, 7.2 m wide $\times$ 7.2 m long $\times$ 1.5 m deep in size, equipped with two 20 inch-in-diameter photomultiplier tubes (PMTs), i.e., HAMAMATSU R3600. The Tibet MD array are made up of 192 muon detectors set up 2.5 m underground. Its total effective area amounts approximately to 10,000 m^2 for muons with energies more than $\sim$ 1 GeV. Our current MC simulation predicts that the cosmic-ray background events will be rejected by approximately 99.99% at

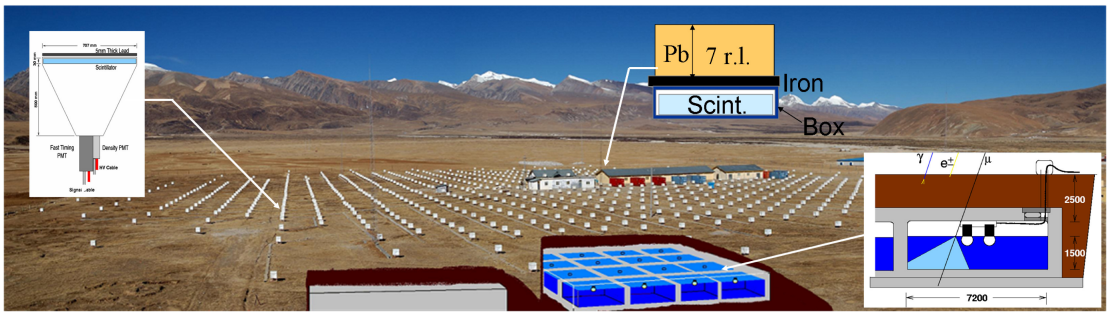

Fig. 14. Schematic view of Tibet (AS+MD+YAC) array.

100 TeV using full-scale (10,000 m^2) MD array. The full-scale MD array will improve the sensitivity to gamma-ray sources by more than an order of magnitude. In 2007, we constructed a prototype water Cherenkov muon detector (approximately 100 m^2) under the existing Tibet air shower array. We have been successfully taking data since December 2007. The preliminary analysis shows that the data is in good agreement with our MC simulation. Now, 5 pools (approximately 4,200 m^2) are under construction as shown in Figure 15.

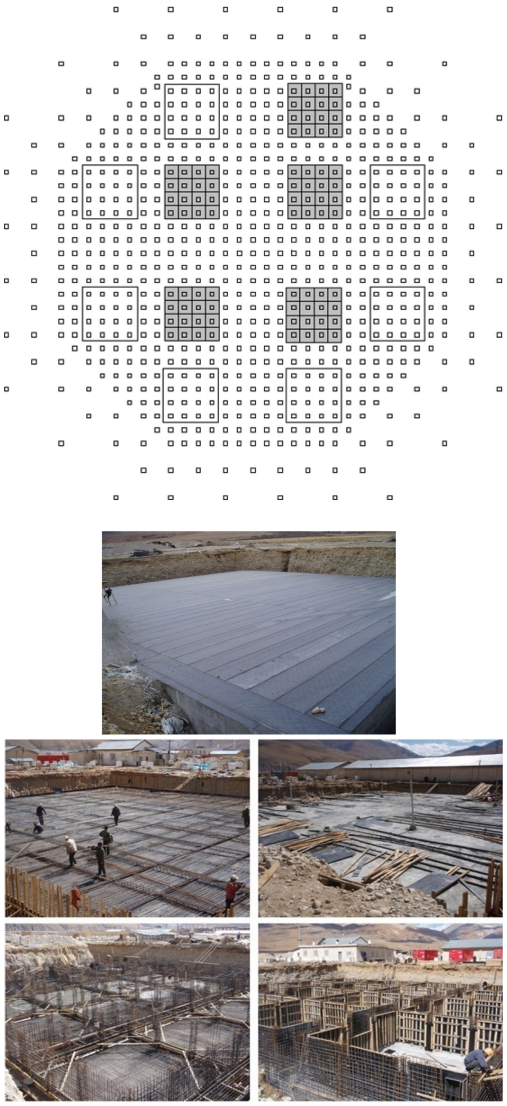

Fig. 15. Schematic view of the Tibet AS+MD array. 5 pools (gray square, approximately 4,200 m^2) are under construction.

The Tibet AS+MD array will have the sensitivity to gamma rays in the 100 TeV region by an order of magnitude better than any other previous existing detectors in the world as shown in Figure 16. We can expect to discover a dozen new point-like sources and diffuse gamma rays from Galactic plane with extremely low background level in the northern sky.

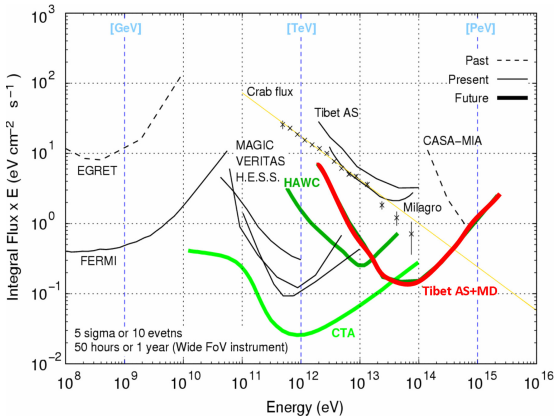

Fig. 16. Integral flux sensitivities to point-like gamma-ray sources.

7.2 Tibet AS+YAC+MD Project

Aiming at the observation of cosmic-ray chemical composition at the knee energy region, a new type air-shower-core detector (YAC, Yangbajing Air shower Core array) has been developed and set up at Yangbajing, 4300 m a.s.l. in Tibet, China since May, 1st, 2009. YAC will work together with the Tibet-III array and a large muon detector as a hybrid experiment. YAC experiment is scheduled in three steps called YAC-I, YAC-II, and YAC-III. YAC-I is a small array consisting of 16 prototype detectors (~10 m^2) located near the center of the Tibet-III array as shown in Figure 17. YAC-I can detect through a few months observation the AS core events of primary energies around 10^{14} eV where mass composition of cosmic rays are known by direct observations [25]. Therefore, the role of YAC-I is to test the interaction models currently used by Monte Carlo (MC) simulations such as QGSJET01, SIBYLL2.1, QGSJET2, EPOS. YAC-II is an array of 124 detectors (~500 m^2) as shown in Figure 18. It is aimed in YAC-II to obtain proton and helium spectra with high statistics in energy range between 50 TeV and several times 10^{15} eV which can be connected with data obtained by direct observations. Finally, YAC-III with large area (400 detectors, ~5000 m^2) is planed to obtain iron spectrum above 10^{15} eV. YAC-I has been already carried out from May, 2009 to February, 2010, and YAC-II has also been started from August 1st, 2011.

Fig. 17. Schematic view of the YAC-I array.

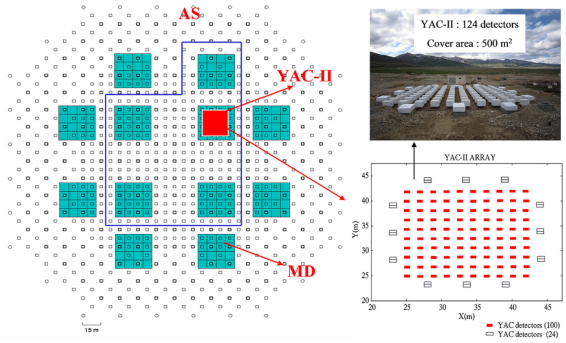

Fig. 18. Schematic view of (Tibet-III+YAC-II+MD) array. The Tibet-III consists of 789 detector units (approximately 36,900 m^2), the YAC-II consists of 124 detector units (approximately 500 m^2), The five MDs (approximately 4,200 m^2) in the blue frame are under construction.

YAC-I detector has the same design of the YAC-II and YAC-III. The only difference between YAC-I, YAC-II and YAC-III is in spacing. Each YAC detector unit consists of lead plates of 3.5 cm (7 r.l.) thick and a scintillation counter which detects the burst size induced by high energy electromagnetic component at the air-shower core. The burst size threshold is set to 100 particles which corresponds to 30 GeV of electromagnetic component incident upon a detector. Wide dynamic range between 1 MIP and 10^6 MIPs (Minimum Ionization Particles) is covered by 2 PMTs (Hamamatsu: R4125 and R5325) as shown in Figure 19. The response linearity of each YAC detector was calibrated by cosmic-ray single muons and by the accelerator beam of the BEPCII (Beijing Electron Positron Collider, IHEP, China).

Tibet-III array consists of 789 detectors, with a covering area about 36900 m^2. An event trigger signal is issued when any four-fold coincidence occurs in detectors recording more than 0.6 particles.The trigger rate is about 680 Hz and the dead time is 15%. Tibet-III is used to measure the arrival direction (θ) and the air shower size (N_e). The angular resolution is about 0.1 degree above 100 TeV and the energy resolution is about 15% at 1 PeV [1]. On-line trigger condition for YAC is "any 1" detector "fired" (the discrimination threshold is about 30 mV). The YAC-II is used to measure the high energy electromagnetic particles in the core region so as to obtain the characteristic parameters of air-shower cores. The inner 100 plastic scintillator units of YAC-II are arranged as an array (10×10 grid) each with an area of 50 cm × 80 cm, with 1.875 m interval; and the outer 24 plastic scintillator units are arranged around the inner array each with an area of 50 cm × 100 cm. The outer 24 units are used to reject non core events whose shower cores are far from the YAC-II array.

Fig. 19. The outlook of YAC detector. Each YAC detector consists of a scintilllator of 80 cm × 50 cm in area with 1 cm thickness and lead absorber of 3.5 cm thickness above the scintillator. Such design provides geometrical uniformity of the detector response within ±6%. A couple of PMTs are used to cover wide dynamic range of the number of particles (burst size) from 1 MIP to 10^6 MIPs.

If one YAC detector unit makes a trigger signal, all ADC data from all YAC units are recorded. Also the trigger signal is sent to the DAQ system for Tibet-III array. ADC pedestal values are measured each 10 minutes. Each DAQ system has GPS clock module independently. The matching between YAC data and Tibet-III data is made using coincidence of GPS clocks and the trigger tag to Tibet-III array.

Our current MC simulation predicts that the performance of YAC-II will be strong enough to separate primary particles into four classes, namely, proton, helium, intermediate nuclei(He< A <Fe), and iron group as shown in Figure 20 where lines are input fluxes and symbols represent estimated distribution by RF (Random Forest algorithm [28]). In 2009, we constructed a prototype YAC detector which is called YAC-I near the center of the Tibet-III air-shower array. We have been successfully taking data from May 2009 to February 2010. The preliminary analysis shows that the data is in good agreement with our MC simulation as shown in Figure 12a, 12b and 12c.

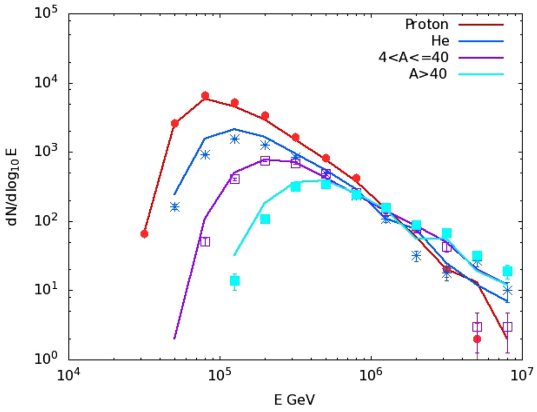

Fig. 20. Separation of AS core events into four classes by YAC-II experiment using RF trained by QGSJET2-MC.

8 Summary

We briefly presented the recent results on high-energy cosmic ray physics obtained using the Tibet-III air-shower array with a characteristic of wide-sky coverage and continuous observation. These results clearly show that the Tibet AS array has capabilities necessary for high-energy particle and gamma-ray astronomy. We also reported the present status of new experiments in which the MD-array and YAC-array are planned to operate together with the AS array. Among this, it is shown that the Tibet AS+MD array has the sensitivity to gamma rays in the 100 TeV region by an order of magnitude better than any other previous detectors existing in the world. We may then have a chance to discover a dozen new point-like gamma-ray sources and also diffuse gamma rays from the Galactic plane with extremely low background level in the northern sky. In addition, the Tibet AS+YAC+MD array enables us to measure the differential energy spectra of primary cosmic-ray components such as protons, helium nuclei, medium nuclei and irons separately in the energy region covering the knee. According to the MC simulation, a full-scale YAC array is powerful enough to study the chemical composition, in particular, to obtain the energy spectrum of the major component around the knee. This work is indispensable to deepen our understanding on the origin and acceleration mechanism of very high energy cosmic rays.

Acknowledgements

The collaborative experiment of the Tibet Air shower Arrays has been performed under the auspices of the Ministry of Science and Technology of China and the Ministry of Foreign Affairs of Japan. This work was supported in part by Grant-in-Aid for Scientific Research on Priority Areas from the Ministry of Education, Culture, Sports, Science and Technology, by Grants-in-Aid for Science Research from the Japan Society for the Promotion of Science in Japan, and by the Grants-in-Aid from the National Natural Science Foundation of China and the Chinese Academy of Sciences (H9291450S3), the Key Laboratory of Particle Astrophysics, Institute of High Energy Physics, CAS. The Knowledge Innovation Fund (H95451D0U2 and H8515530U1) of IHEP, China and the project Y0293900TF of NSFC also provide support to this study.

References

[1] M. Amenomori, et al., 2008, ApJ, 678, 1165
[2] M. Amenomori, et al., 2009, ApJ, 692, 61
[3] M. Amenomori, et al., 2006, Science, 314, 439
[4] A. A. Abdo, et al., 2009, Science, 325, 840
[5] J. L. Zhang, 2003, ICRC, 4, 2405
[6] J. L. Zhang, 2005, ICRC, 4, 93
[7] M. Amenomori, et al., 2010, ApJ, 709, L6
[8] E. G. Berezhko and L. G. Ksenofontov, 1999, J. Exp. Theor. Phys., 89, 391
[9] V. S. Ptuskin, et al., 1993, A&A, 268, 726
[10] A. D. Erlykin and A. W. Wolfendale, 2005, Astropart. Phys., 23, 1
[11] S. I. Nikolsky and V. A. Romachin, 2000, Phys. Atom. Nucl., 63, 1799
[12] M. Shibata, et al., 2010, ApJ, 716, 1076
[13] K. Kawata, 2011, ICRC, 11, 241
[14] NOAA/NGDC, Sunspots numbers, 2010, http://www. ngdc.noaa.gov/stp/stp.html
[15] Wilcox Solar Observatory, WSO Computed "Tilt Angle" of the Heliospheric Current Sheet, 2010, http://wso. stanford.edu/Tilts.html
[16] G. Guillian, et al., 2007, Phys. Rev. D, 75, 0620031
[17] T. Sako, 2011, ICRC, 11, 105
[18] D. Gurnett, et al., 2006, AIPC, 858, 129
[19] R. Lallement, et al., 2005, Science, 307, 1447
[20] P. Frisch, 1996, Space Sci. Rev., 78, 213
[21] J. Heerikhuisen, et al., 2010, ApJ, 708, L126
[22] K. Munakata, et al., 2010, ApJ, 712, 1100
[23] M. Amenomori, et al., 2010, ApJ, 711, 119
[24] X.-B. Qu, et al., 2011, ICRC, 6, 281
[25] H. S. Ahn, et al., 2010, ApJ, 714, L189
[26] F. A. Aharonian, et al., 2005, Science, 307, 1938
[27] M. Takita, 2011, ICRC, 6, 336
[28] L. Breiman, http://www.stat.berkeley.edu/∼breiman/RandomForests/cc-papers.htm